A highly oxidized ferrian salite-, kennedyite-, forsterite-, and rhönite-bearing alkali gabbro from Kauai, Hawaii and its mantle xenoliths[1]

A. Dana Johnston[2] and James H. Stout

Department of Geology and Geophysics

University of Minnesota, Minneapolis, Minnesota 55455

Abstract

Three types of rock, each with unusually oxidized mineral assemblages, are found in close association as part of a probable feeder pipe to the alkalic lavas on Kauai, Hawaii. The first type is an alkali gabbro consisting of potassic oligoclase (66% by volume), ferrian salite (27%), kennedyite (3%), magnesioferrite (3%) and trace amounts of rhönite, kaersutite, apatite, hematite and nearly pure forsterite. Electron microprobe analyses of these phases show them to be exceptionally enriched in Mg and ferric iron. These data combined with textural observations demonstrate that the alkali gabbro melt existed in a highly oxidized state prior to the onset of crystallization and that this condition prevailed throughout the course of crystallization.

The second lithologic type consists of an assortment of mantle xenoliths, mostly spinel lherzolites, that were entrained by the alkali gabbro at depth prior to its crystallization. There was extensive development of oxidation symplectites within the primary grains in the outer two cm of the xenoliths. Original mantle olivine (Fo_{88-91}) has oxidized to form bleb-like intergrowths of orthopyroxene (En_{94}) and magnesioferrite (Mt_{58}) in a more magnesian (Fo_{95}) olivine host. Comparison of these data with relevant 1 atm experimental data in the system $MgO–FeO–Fe_2O_3–SiO_2$ indicates conditions of 10^{-3} fo_2 and 1165°C for the formation of these symplectites.

The third lithologic type is referred to here as the fine-grained groundmass. Like the alkali gabbro, the fine-grained groundmass has a high Fe^{3+}/Fe^{2+} but consists only of ferrian salite (62%), potassic oligoclase (17%), forsterite (14%), magnesioferrite (7%) and trace amounts of apatite. The gradational contacts of the fine-grained groundmass with the xenoliths and comparative microprobe analyses suggest that the groundmass liquid was derived in part from the xenoliths by partial melting, and the subsequent crystallization of that liquid was complete prior to the introduction of the alkali gabbro. The formation of the oxidation symplectites is closely associated with the fine-grained groundmass and hence the melting event, and appears to have been prior to alkali gabbro intrusion.

Introduction

The determination of the chemical and mineralogic composition of the earth's mantle and its pressure and temperature distribution is essential in understanding the origin of the compositionally diverse liquids observed at the surface. Direct sources of data that bear on the problem include xenoliths of presumed mantle origin and the igneous rocks that bring them to the surface. A large and growing body of evidence based on various mineral geothermometers and geobarometers indicates that many xenoliths have equilibrated in the temperature range 1000–1300°C corresponding to mantle depths on the order of 70 to 100 km. Their enclosing melts must have originated from at least those depths.

More specific information on the original environment of the melts is difficult to obtain. It is well known that pressure, temperature, and the fugacities of various volatile components are important variables, but it is less certain to what extent their initial values are retained upon eruption. Estimates of fo_2 range from very reducing (*e.g.*, Sato, 1972) to very oxidizing (*e.g.*, Powell, 1978) at magmatic temperatures although most extrusive rocks yield fo_2 values near the fayalite–quartz–magnetite buffer reaction (Haggerty, 1976). There is both textural and mineralogic evidence that some melts have undergone oxidation during eruption (Sato, 1972; Gerlach and Nordlie, 1975a,b; Wright and Okamura, 1977) whereas others

appear to have experienced reduction (Anderson, 1968).

It is our purpose here to present a general description of an alkali gabbro that appears to have had an unusually high oxygen content prior to the entrapment of a suite of spinel lherzolite xenoliths and during subsequent crystallization. The rocks are located on the south side of the island of Kauai, Hawaii, just north of the town of Kalaheo along the east side of Puuwai Road, 150 m south of its intersection with Kikala Road. The area was mapped (MacDonald *et al.*, 1960, Palmiter, 1975) as a small subcircular plug approximately 200 m in diameter which intrudes the Pleistocene Koloa Volcanic Series. The latter rocks are predominantly alkali basalt and olivine nephelinites which overlie the Pliocene tholeiitic lavas of the Waimea Canyon Volcanic Series. Just across the valley along the west side of Kikala Road there are many small (<2 m) rounded boulders of xenolith-free ijolite. Based on geologic mapping, MacDonald *et al.* (1960) and Palmiter (1975) proposed that the ijolite may represent the core of the plug, and the alkali gabbro a marginal facies.

Because the plug is younger than the Pleistocene Koloa Series which it intrudes, the plug probably represents a remnant of a feeder pipe to the upper part of the post-erosional alkalic lavas now removed by erosion. Supporting this interpretation is the location of the plug along an approximately N10°E trending array of Koloa Series vents described in MacDonald *et al.* (1960). It is generally thought that the nephelinitic magmas of the younger Koloa Series originate at depths of at least several tens of kilometers whereas the older tholeiitic suite (Waimea Canyon Series) originated in relatively shallow magma chambers. There are apparently no other established outcrops of alkali gabbro on Kauai.

Rock description

Observations reported in this study are based on sixteen large specimens collected by JHS in 1977 and twenty-five specimens collected by ADJ in 1982. All specimens are exceptionally hard and fresh and are distinguished by the presence of large (3–18 cm) coarse-grained spinel lherzolite (with rare orthopyroxenite, clinopyroxenite and dunite) xenoliths within a groundmass of alkali gabbro. The xenoliths comprise 60–70 volume percent of all samples and although usually well-rounded, some are angular. All are rich in olivine (85%) with less orthopyroxene (10%), clinopyroxene (4%) and Cr-spinel (1%). Distinctive black rims (up to 2 cm thick) containing an oxidation symplectite occur on all xenoliths. In smaller xenoliths the oxidation assemblage is present throughout. White (1965) described abundant lherzolite with lesser dunite and orthopyroxenite xenoliths from the same locality. He also described the black rims and ascribed them to high temperature oxidation.

In detail, the host rock actually consists of two textural and mineralogic types. The first is a coarse-grained (2–5 mm) alkali gabbro that brought the xenoliths to the near surface. Its modal composition is potassic oligoclase, 66%; ferrian salite, 27%; kennedyite, 3%; magnesiofer-

rite, 3%; and trace amounts of rhönite, kaersutite, and apatite. Trace amounts of an exceptionally magnesian olivine (Fo_{98}) up to 3 mm in length are also present.

The second type is hereafter referred to as the fine-grained groundmass. Its texture is finer (0.3–0.5 mm) than the alkali gabbro and consists of ferrian salite (62%), oligoclase (17%), forsterite (14%), magnesioferrite (7%) and apatite (tr). Kennedyite, kaersutite, and rhönite are absent. A notable feature of both rock types, particularly the fine-grained groundmass, is the presence of vesicular cavities lined with euhedral crystals of ferrian salite, apatite and oligoclase. Late stage zeolites (described in detail by White (1965)) and pods of concentrically layered carbonate are also present.

Usually the fine-grained groundmass entirely covers the xenolith surfaces but in some cases the contact between them is truncated by the alkali gabbro such that the latter is in direct contact with xenolith. In no cases were oxidation symplectites observed that could be attributed to the effects of the alkali gabbro. In some cases the fine-grained groundmass fills the gap between adjacent xenoliths, sometimes defining a uniformly curved miniscus between them. In other cases there is evidence, in the form of relict xenolith outlines, that volume once occupied by xenoliths is now occupied by fine-grained groundmass. The relict outlines are delineated by a remarkably uniform curved layer of adjoining magnesioferrite euhedra (Fig. 1). In xenoliths with embayments filled by fine-grained groundmass, the oxidized rims follow the outline of the embayments and thus appear unrelated to either the original nodule shape or the alkali gabbro enclosing them.

The alkali gabbro, where in contact with either fine-grained groundmass (Fig. 1) or xenoliths, is marked by a continuous string of large magnesioferrite crystals which appears to have nucleated on those surfaces. An adjacent, almost continuous layer of large (up to 1 cm) ferrian salite phenocrysts occurs within the gabbro and also appears to have nucleated in that position during crystallization.

Methods

Samples for whole rock analyses of the groundmasses were prepared by grinding a large sample to approximately 10 mesh and then hand picking under a binocular microscope about 7 grams of each of the fine-grained groundmass and alkali gabbro. The two are easily distinguishable and as such we have confidence in the purity of the separates. The sample for the xenolith rim analysis was prepared by cutting a 2 cm thick slab through a large whole xenolith and then sawing off a sample of the distinctive black rim taking care that the cut was well within the rim on both sides of the slab. The sample for the xenolith-core analysis was taken from the same slab making sure the sample was closer to the center of the xenolith than where the rim appeared to stop. The sample for the whole xenolith analysis was prepared from a separate, egg-shaped xenolith which was removed intact from the groundmasses.

Microprobe analyses reported here (Tables 2, 3 and 4) were done by JHS at the University of Bergen, Norway and by ADJ at
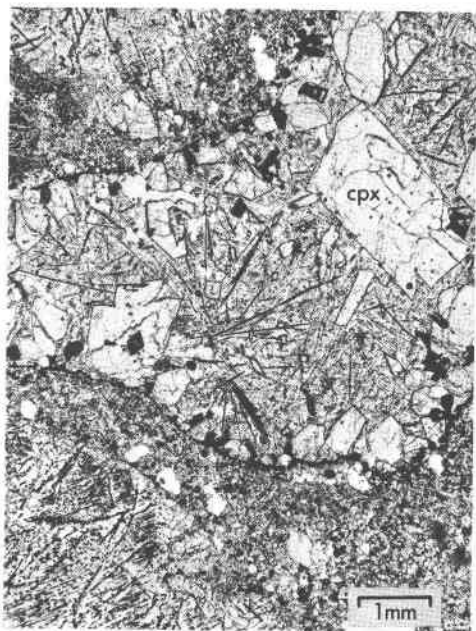
Fig. 1. Low magnification photomicrograph illustrating the gradational contacts between xenoliths (upper and lower left) and the granular fine-grained groundmass. Sharp contacts between the fine-grained groundmass and the alkali gabbro (center) are marked by a continuous string of magnesioferrite grains. Alkali gabbro phenocrysts include ferrian salite (cpx) and magnesioferrite euhedra (equant black grains) in a quenched groundmass of kennedyite (needle-like black grains) and oligoclase.

Phillips Petroleum Company, Oklahoma. Operating conditions for the Bergen analyses were 15 kV accelerating potential, sample currents of 5 or 10 nA (on brass), and a beam diameter of approximately 2 μm. A defocused beam was used to minimize volatilization of alkali metals in the feldspars. X-ray counting times were 40 sec on peaks and 5 sec on backgrounds. Standards consisted of natural minerals, synthetic oxides, and pure metals. Data reduction and ZAF corrections were applied using the automated Magic IV subroutine. Typical standard deviations of determined weight percent oxides are <1% of the amount present for oxides present in excess of 5 wt.%; 2–5% for oxides present in the range 1–5 wt.%; and 10–30% of the amount present for oxides present in amounts <1 wt.%.

Operating conditions for the Phillips analyses were 20 kV accelerating potential, beam currents of 15–16 nA and a beam diameter of 2 μm. The beam current was measured with a Faraday cup before each analysis and counts on standards and samples were normalized to a counts per second per nA beam current basis. Counts were collected on peaks for a minimun of 10 s and a maximum of 30 sec. If a standard deviation of 1% was achieved before 30 sec, counting stopped. Backgrounds were counted for 5 sec. Natural mineral standards were used and the data were reduced using an automated ZAF program. Standard deviations are comparable to those quoted for the Bergen analyses.

An estimate of the ferric iron content can be calculated from an electron microprobe analysis on the basis of the ideal number of anions using $Fe^{3+} = 2$(ideal # anions −((ideal # anions)(ideal # cations)/(calculated # cations))). Alternatively, for analyses

calculated on the basis of the ideal number of cations, identical values for ferric iron are calculated by $Fe^{3+} = 2$ (ideal # anions − calculated # anions) where the calculated number of anions is the sum of the oxygen equivalents of the cations calculated assuming all iron is ferrous. In this study, ferric iron has been calculated by the second method bacause an estimate of the uncertainty of the method was made by Finger (1972). Comparison of ferrian salite analyses (this study) recalculated in this way with wet chemical analyses of ferrian salites from the same locality given by White (1965) shows good agreement.

Molecular components of mineral analyses were calculated using a matrix transformation from cations per formula unit. This method is discussed by Greenwood (1975) and Brady and Stout (1980) and is completely general in the sense that any choice of independent components may be made depending on the problem to be solved. Negative coefficients for some components are occasionally calculated. They simply indicate that the composition being considered falls outside the composition space enclosed by the chosen molecular components. Modes for the alkali gabbro and the fine-grained groundmass were likewise calculated by a matrix transformation.

Bulk rock chemistry

The alkali gabbro (analysis 1, Table 1) of this study has exceptionally high Fe^{3+}/Fe^{2+} (14.5, atom units) and an unusually high alkali content ($Na_2O + K_2O = 8.45$ wt.%). On an alkali-silica diagram, analysis 1 plots well within the alkalic field and considerably on the alkali-rich side of the alkalic trend as defined for Hawaiian volcanics by MacDonald (1968). The only other reported case known to us of rocks similar to the alkali gabbro is from Kilbeinsey Island, north of Iceland (Sigurdsson and Brown, 1970). Analysis 2 (Table 1) is from their paper and shows higher Fe^{3+}/Fe^{2+} (21.3, atom units) and lower total

Table 1. Whole rock analyses

	1	2	3	4	5	6
SiO_2	50.03	50.29	42.06	43.45	42.34	41.55
Al_2O_3	15.47	16.08	8.66	0.81	1.05	0.98
TiO_2	2.82	0.66	1.85	0.01	0.05	0.09
Fe_2O_3	6.49	8.98	12.04	1.15	4.50	4.31
FeO	0.40	0.38	1.22	7.06	4.38	5.54
MgO	5.68	8.18	18.85	44.65	44.87	43.81
MnO	0.16	0.17	0.20	0.14	0.15	0.14
CaO	8.51	12.79	11.13	1.08	1.22	1.31
Na_2O	5.76	2.37	2.30	0.03	0.16	0.18
K_2O	2.69	0.04	0.66	0.01	0.05	0.07
P_2O_5	1.04	0.06	0.54	0.02	0.25	0.08
Cr_2O_3	n.d.	n.d.	n.d.	n.d.	n.d.	0.42
NiO	n.d.	n.d.	n.d.	n.d.	n.d.	0.25
H_2O^+	0.36	n.d.	0.32	0.40	0.32	0.61
H_2O^-	0.08	n.d.	0.20	0.05	0.14	0.24
CO_2	0.05	n.d.	0.30	0.32	0.30	0.15
Total	99.54	100.00	100.33	99.16	99.78	99.73

n.d.: not determined
1. Alkali gabbro, this study, specimen JS-HK-3
2. Forsterite-enstatite basalt, Kolbeinsey Island (Sigurdsson and Brown, 1970, p. 210)
3. Fine-grained groundmass, this study, specimen JS-HK-3
4. Xenolith core, this study, specimen JS-HK-6
5. Xenolith rim, this study, specimen JS-HK-6
6. Whole xenolith, this study, specimen JS-HK-9

Analyses performed either by M. Ramlal, University of Manitoba or by Scienterra, Inc., (Spokane, WA); with P_2O_5 by spectro-photometry, H_2O, CO_2, and FeO by wet chemistry, and all others by atomic absorption or x-ray fluorescence.

Table 2. Microprobe analyses of sector-zoned ferrian salite in the alkali gabbro

	1 Z6	2 Z1	3 Z5	4 Z2
SiO_2	44.17	42.63	43.75	40.77
Al_2O_3	6.93	8.24	7.32	9.75
TiO_2	2.48	4.92	2.60	6.31
FeO*	9.48	7.87	9.51	7.92
MgO	11.92	11.25	12.10	10.24
MnO	0.11	0.15	0.13	0.19
CaO	22.15	22.03	22.30	21.38
Na_2O	0.59	1.26	0.58	1.51
Cr_2O_3	0.08	0.01	0.00	0.00
Total	97.91	98.35	98.29	98.08
FeO***	2.42	1.13	1.70	2.60
Fe_2O_3***	7.85	7.48	8.67	7.03
Total***	98.70	99.10	99.16	98.78
Si	1.684	1.617	1.660	1.557
Al	0.311	0.368	0.327	0.439
Ti	0.071	0.140	0.074	0.181
Fe^{2+}	0.077	0.036	0.054	0.051
Fe^{3+}	0.225	0.214	0.248	0.202
Mg	0.677	0.636	0.684	0.583
Mn	0.003	0.005	0.004	0.006
Ca	0.904	0.895	0.906	0.875
Na	0.044	0.093	0.043	0.112
Cr	0.002	0.000	0.000	0.000
Total	4.000	4.000	4.000	4.000
Number of oxygens	6	6	6	6
NaFe^{3+}Si_2O_6 (Ac)	4.4	9.3	4.3	11.2
CaTiAl_2O_6 (Tp)	7.1	14.0	7.4	18.1
CaFe^{3+}AlSiO_6 (FATs)	18.1	12.1	20.5	8.7
CaAl_2SiO_6 (CATs)	-0.6	-1.1	-1.3	0.2
CaFe^{2+}Si_2O_6 (Hd)	7.7	3.6	5.4	5.1
CaMgSi_2O_6 (Di)	58.1	60.9	58.6	55.1
Mg_2Si_2O_6 (En)	4.8	1.3	4.9	1.6
SiO_2 (Qz)	0.9	-0.6	0.4	-1.2
SECTOR	{100} core	{100} rim	{010} core	{010} rim

* Total Fe as FeO; *** based on calculated Fe^{2+} and Fe^{3+}.

core analyses of the same xenolith are similar. Total iron is nearly the same.

Groundmass petrography and mineral chemistry

In this section we report petrographic data from both the alkali gabbro and the fine-grained groundmass. Tables 2 and 3 give microprobe analyses of phases from the alkali gabbro exclusively and are intended to illustrate the compositional ranges we observe.

Ferrian salite

Pleochroic canary yellow (in thin section) clinopyroxene is an abundant phase in both the alkali gabbro and fine-grained groundmass. In the alkali gabbro, elongate euhedra of ferrain salite with cross-sectional diameters of up to 0.8 mm and lengths of up to 1.0 cm occur, whereas in the fine-grained groundmass ferrian salite occurs as euhedral, approximately equant grains with an average grain size of 0.075 mm. Euhedral kaersutite forms epitaxial overgrowths on some ferrian salite grains.

Spectacular sector zoning is ubiquitous in the ferrian salite phenocrysts in the alkali gabbro. In addition, virtually all grains show strong concentric zoning within individual sectors.

Spot analyses of core and rim compositions of a {100} and an adjacent {010} sector in a single euhedral phenocryst are given in Table 2. These analyses are recalculated to a set of end member components which includes ferri-aluminum Tschermaks (FATs), calcium aluminum Tschermaks (CATs), and titanpyroxene (Tp) in order to facilitate comparison to synthetic systems studied by Akasaka and Onuma (1980) and Onuma *et al.* (1981). Because the number of components (8) in the original oxide analyses is greater than the chosen number of pyroxene endmembers (7), an arbitrary dummy component, chosen here as SiO_2, is necessary for an exact solution of the matrix transformation. The magnitude of this component is small and in general appears to be within the limits of cumulative analytical error. In an ideal pyroxene analysis, components other than stoichiometric pyroxenes must have zero coefficients.

In the system Di–CaTs–FATs, Onuma *et al.* (1981) found that the FATs content of clinopyroxenes is strongly dependent on the oxygen fugacity and independent of pressure. The fact that the FATs content of the Kauai pyroxenes decreases from core to rim suggests that the oxygen fugacity of the alkali gabbro melt may have decreased during crystallization. This interpretation is complicated, however, by the presence of an acmite component which increases from core to rim. Apparently as Na^+ became enriched in the liquid during crystallization, Fe^{3+} was taken up as acmite thus reducing the FATs content of the pyroxene rims relative to their cores. Moreover, Onuma *et al.* (1981) showed that the solubility of total Tschermak's components in diopside is enhanced

alkalies (Na_2O + K_2O = 2.4 wt.%) than the alkali gabbro of this study. They report phenocryst phases of ferrian augite, nearly pure forsterite, and enstatite that are similar to those of the alkali-gabbro. Although Sigurdsson and Brown suggest that the high oxidation state may have been caused by infiltration of sea water, the very low $^{87}Sr/^{86}Sr$ of 0.70290 reported by O'Nions and Pankhurst (1974) seems to preclude this possiblity.

Analysis 3 is of the fine-grained groundmass of the present study. On an alkali-silica diagram, it too plots well within the alkali field, close to the intersection of the nephelenitic and alkalic trends and near the origins of both (MacDonald, 1968). The ferric/ferrous ratio is abnormally high (8.9, atomic units) but lower than in the alkali gabbro. Similarly, total alkalies (Na_2O + K_2O = 3.0 wt.%) are less than in the gabbro. The exceptionally high MgO and low SiO_2 demonstrate its picritic affinities and primitive nature.

Analyses 4–6 (Table 1) are of the spinel lherzolite xenoliths of this study. Analyses of the core (analysis 4), and the rim containing the oxidation symplectite (analysis 5) of the same xenolith and of a different whole xenolith (analysis 6) are presented. Apart from a much higher ferric to ferrous iron ratio in the rim analysis, the rim and

Table 3. Microprobe analyses of phases in the alkali gabbro

	Kennedyite			Magnesioferrite			Hematite	Oligoclase	Kaersutite	Rhönite	Forsterite
	1	2	3	4	5	6	7	8	9	10	11
SiO_2	0.15	0.16	0.00	0.30	0.11	0.18	0.02	62.68	38.39	30.95	42.73
Al_2O_3	1.82	1.99	1.95	9.13	8.51	9.09	0.79	22.00	11.79	13.19	0.06
TiO_2	46.22	48.97	50.37	2.01	2.39	2.75	18.80	0.21	8.95	5.10	0.04
FeO^*	40.80	37.53	37.54	63.55	64.47	65.36	67.21	0.83	8.18	17.31	2.04
MgO	5.19	6.25	6.64	16.31	16.51	16.16	6.57	0.00	13.46	18.99	54.72
MnO	0.54	0.32	0.16	1.87	1.97	1.28	0.32	0.04	0.14	0.34	0.59
CaO	0.04	0.07	0.02	0.00	0.01	0.03	0.04	3.25	10.86	8.79	0.09
Na_2O	0.00	0.00	0.03	0.05	0.02	0.00	0.00	7.16	2.89	2.75	0.00
K_2O	0.00	0.00	0.02	n.d.	n.d.	0.00	n.d.	1.78	0.90	0.04	0.02
Cr_2O_3	0.09	0.01	0.06	0.00	0.00	0.05	0.00	0.03	0.03	0.00	0.02
Total	94.85	95.30	96.79	93.22	93.98	94.90	93.75	97.98	95.59	97.46	100.31
FeO^{***}	0.22	0.64	0.42	7.53	7.49	9.55	4.81	**	**	1.74	**
$Fe_2O_3^{***}$	45.10	40.99	41.25	62.25	63.31	62.02	69.34	**	**	17.30	**
$Total^{***}$	99.37	99.40	100.92	99.45	100.32	101.11	100.69	**	**	99.19	**
Si	0.006	0.006	0.000	0.100	0.003	0.006	0.000	2.834	5.765	4.005	1.008
Al	0.081	0.087	0.084	0.352	0.326	0.346	0.023	1.173	2.088	2.012	0.002
Ti	1.312	1.374	1.390	0.049	0.059	0.067	0.347	0.007	1.010	0.496	0.001
Fe^{2+}	0.007	0.020	0.013	0.206	0.204	0.258	0.099	0.032	1.028	0.189	0.040
Fe^{3+}	1.281	1.151	1.139	1.532	1.551	1.507	1.282	0.000	**	1.685	**
Mg	0.292	0.347	0.363	0.795	0.801	0.778	0.241	0.000	3.012	3.663	1.925
Mn	0.017	0.010	0.005	0.052	0.054	0.035	0.007	0.001	0.018	0.037	0.012
Ca	0.002	0.003	0.001	0.000	0.000	0.001	0.001	0.158	1.747	1.218	0.002
Na	0.000	0.000	0.002	0.003	0.001	0.000	0.000	0.628	0.841	0.690	0.000
K	0.000	0.000	0.001	n.d.	n.d.	0.000	n.d.	0.102	0.173	0.006	0.001
Cr	0.003	0.000	0.002	0.000	0.000	0.035	0.000	0.001	0.003	0.000	0.000
Cation Total	3.000	3.000	3.000	3.000	3.000	3.000	2.000	4.937	15.686	14.000	2.991
# Oxygens	5	5	5	4	4	4	3	8	23	20	4

n.d.: not determined; *: total Fe as FeO; **: not calculated; ***: based on calculated Fe^{2+} and Fe^{3+}.

by oxygen fugacities greater than the magnetite–hematite buffer whereas the FATs component will break down to CaTs plus other phases at low oxygen fugacity. The high total Tschermak's components in the ferrian salite phenocrysts (Table 2) (FATs + Tp = 25 mole%) and the virtual absence of any CATs component suggests that highly oxidizing conditions prevailed during the entire course of ferrian salite crystallization.

Spectroscopic studies by Bell and Mao (1971) of ferrian salite crystals from Kolbeinsey Island near Iceland and from Tugtutog, Greenland show a strong absorption band attributed to charge transfer between octahedrally coordinated Fe^{3+} and the coordinating ligand, oxygen. This absorption band trails into the visible region and gives rise to the yellow color in ferrian salites (Bell and Mao, 1971). The band is not observed in lunar clinopyroxenes, which contain only Fe^{2+}, and is therefore attributed solely to Fe^{3+}. The significant amounts of Ti (up to 3.1 wt.%) in the samples studied by Bell and Mao cause no visible absorption, suggesting that Ti^{4+} is the dominant titanium species. When present in oxygen compounds, Ti^{4+} alone causes no absorption in the visible region (Marfunin, 1979). Moreover, the Kolbeinsey Island sample exhibits a weak absorption band beyond the visible region which is attributed to octahedrally coordinated Fe^{2+} (Bell and Mao, 1971). Similar studies of ferrian salite

crystals from the present study (G. R. Rossman, pers. comm., 1980) show them to be spectroscopically similar to those from Kilbeinsey Island. Thus the yellow color of the Kauai ferrian salites, if indeed due to the charge transfer mechanisms suggested by Bell and Mao (1971), indicates that much of the titanium is Ti^{4+} and much of the iron is Fe^{3+}.

Magnesioferrite

This phase occurs in both the alkali gabbro and the fine-grained groundmass. In the alkali gabbro it occurs as small (0.3 mm), frequently skeletal euhedra whereas in the fine-grained groundmass, magnesioferrite occurs as smaller (0.1 mm), usually anhedral grains. This phase also commonly occurs as perfect euhedra totally enclosed in ferrian salite phenocrysts. Magnesioferrite was one of the earliest phases to crystallize in the alkali gabbro, probably second to olivine. In reflected light, the vast majority of the magnesioferrite grains appear homogeneous and lack exsolution although in a few grains, a rhombohedral Fe–Ti–Mg oxide is observed.

Analyses 4 and 5 (Table 3) are of the core and rim, respectively, of a euhedral magnesioferrite grain in the alkali gabbro. These analyses are virtually identical, demonstrating that compositional zoning is minimal. These analyses transform into the following set of end-

Fig. 2. Photomicrograph illustrating the texture of the alkali gabbro. Euhedral ferrian salite crystals (cpx) and a forsterite crystal (ol) with swallow-tail terminations are shown. Kennedyite (kd) occurs as linear en-echelon aggregates. The groundmass consists of oligoclase.

member components in mole percent: $MgFe_2O_4$ (mf), 62; $MgAl_2O_4$ (sp), 17; $FeFe_2O_4$ (mt), 14; Fe_2TiO_4 (usp), 4; Mn_2TiO_4, 2. Analysis 6 (Table 3) is of a somewhat skeletal magnesioferrite grain from the alkali gabbro which contains minor Mg–Ti-hematite. Analysis 7 (Table 2) is of the Mg–Ti hematite referred to above and transforms to 64 mole% Fe_2O_3 (Hm), 24% $MgTiO_3$ (Gk), 10% $FeTiO_3$ (Ilm), 1.1% Al_2O_3, and 0.7% $MnTiO_3$.

Kennedyite

Kennedyite, an intermediate member in the pseudobrookite series $Fe_2^{3+}TiO_5$–$MgTi_2O_5$ (von Knorring and Cox, 1961) occurs exclusively in the alkali gabbro as linear en-echelon aggregates of extremely thin (10 μm) orange-brown tabular blades (Fig. 2). In reflected light, kennedyite appears homogeneous, somewhat skeletal, and lacks exsolution. Positive identification of this phase was accomplished with a Gandolfi camera X-ray photograph (D. T. Griffen, pers. comm. 1979). Textural evidence indicates that kennedyite crystallized after olivine, magnesioferrite, and probably after ferrian salite but prior to the dominantly feldspathic groundmass. There is no doubt that this phase formed by primary magmatic crystallization.

Three spot analyses (Table 3, analyses 1–3) illustrate the range in observed compositions of kennedyite in this study. The ranges in mole percent molecular components are: $MgTi_2O_5$, 29–36; $Fe_2^{3+}TiO_5$, 57–64; Al_2TiO_5, 4; $Fe^{2+}Ti_2O_5$, 0.7–2.0; $MnTi_2O_5$, 0.5–1.7.

Forsterite

Nearly pure forsterite occurs in both the alkali gabbro and the fine-grained groundmass. In the alkali gabbro it occurs as rare, large (3 mm) phenocrysts usually with swallow tail terminations (Fig. 2). In cross section, these crystals are invariably hollow. The distinctive shape of these crystals and the absence of oxidation symplectite demonstrates that these olivines originated by crystallization from the alkali gabbro liquid rather than by being liberated from xenolith rims.

In the fine-grained groundmass, small (up to 0.3 mm), equant, euhedral to anhedral forsterite grains are abundant, but it is not clear that they have crystallized directly from a melt. These grains lack the oxidation symplectite that is characteristic of olivine from xenolith rims. They are similar, however, to clear, highly magnesian olivine associated with high silica glass in interstitial melt regions of the xenoliths (Stout and Johnston, 1980). The fine-grained groundmass olivine commonly contains tiny inclusions of probable magnesioferrite, ferrian salite, and/or glass.

Analysis 11 (Table 3) is of the rim of a large skeletal forsterite phenocryst in the alkali gabbro. This analysis recalculates to Fo_{98}. The core of this grain has essentially the same mole percent forsterite but contains more CaO (0.24 wt.%) and less MnO (0.40 wt.%).

Kaersutite

This phase occurs exclusively in the alkali gabbro, as either tiny (0.07 mm) euhedral microphenocrysts or as euhedral to spicular epitaxial overgrowths on ferrian salite crystals. Analysis 9 (Table 3) is representative. Ferric iron cannot be calculated in amphiboles unless a total number of cations, between 15 and 16, is specified. Further complications involve the possibility that some of the OH^-, Cl^-, or F^- may have been replaced by oxygen, as is the case in oxy-hornblendes. This substitution is commonly compensated by oxidation of Fe^{2+} to Fe^{3+} and seems probable in the Kauai kaersutites given the highly oxidized nature of the alkali gabbro. Because of these stoichiometric uncertainties, Fe^{3+} was not calculated. It is likely though that much of the iron is Fe^{3+}. Titanium is exceptionally abundant in this phase, comprising one atom per half unit cell. The substantial aluminum is entirely tetrahedral.

Rhönite

This phase, like the kaersutite, occurs only in the alkali gabbro as tiny, commonly skeletal, euhedral microphenocrysts or as euhedral epitaxial overgrowths on ferrian salite crystals. Rhönite and kaersutite are easily mistaken for each other as both have relatively deep absorption and prismatic form. The analyses reported by White (1965, p. 133) from the alkali gabbro, described as an "amphibolelike mineral", contain 25–32 wt.% SiO_2 and are almost certainly of rhönite.

Considerable range in composition exists in the Kauai rhönites and analysis 10 represents an intermediate composition. The Fe^{3+}/Fe^{2+} ratio of 8.9 in our analysis 10 (Table 3) contrasts greatly with values of 0.92 or less in the rhönite analyses from Deer *et al.* (1978). Additionally, the Kauai rhönites are considerably more magnesian (3.7 atoms/14 cations versus <2.9) and sodic and less calcic than those in Deer *et al.* (1978) Although analysis 10 (Table 3) has less Ti than the analyses in Deer *et al.* (1978) other analyses of the Kauai rhönites yield comparable TiO_2.

Rhönite is a relatively rare mineral, typically found in undersaturated alkaline mafic rocks (Cameron *et al.*, 1970; Magonthier and Velde, 1976). The stability of rhönite extends to at least 1320°C (Grandclément, 1980) and appears independent of fo_2 between NNO and IW buffers between 1150–1250°C (Boivin, 1980). Rhönite appears stable to at least 2 kbar total pressure (Grandclément, 1980).

Oligoclase

Potassic oligoclase accounts for approximately 65 volume percent of the alkali gabbro. This phase is less abundant in the fine-grained groundmass, comprising roughly 17 volume percent. In the alkali gabbro the oligoclase typically occurs in radial splays which are typical quench textures. The lath interiors usually contain abundant sub-micron inclusions of probable hematite arranged sub-parallel to the elongation direction of the lath giving them a feathery appearance. Textural evidence indicates that oligoclase was the last phase to crystallize.

A representative analysis of oligoclase is given in Table 3, analysis 8. The low oxide total probably indicates that some alkali metal migration did occur during analysis in spite of using a defocused electron beam. The analysis recalculates as 71 mole% albite, 18 mole% anorthite, and 11 mole% K-feldspar, placing it approximately on the oligoclase–anorthoclase boundary in a ternary feldspar plot. All feldspar analyses from the Kauai specimens contain considerable Fe (up to 1.8 wt.% FeO*), which is largely present as the minute hematite inclusions noted in thin section.

Apatite

Apatite is an abundant accessory phase in the alkali gabbro, typically found as small skeletal crystals. It also occurs with ferrian salite and oligoclase projecting into vesicles, and as small needles totally enclosed in ferrian salite crystals. Energy dispersive spectra of the apatite reveal only Ca and P.

Spinel lherzolite petrography and mineral chemistry

Mantle xenoliths (2–12 cm across) make up 60–70 volume percent of all rocks studied. Nearly all (95%) of these are coarse spinel lherzolite, and in this section we describe their petrography and mineral chemistry.

Olivine

Olivine is the most abundant phase, and because of the compositional and textural effects of the peripheral oxidation symplectites, we distinguish between olivine in the cores of xenoliths and olivine containing the symplectites near the rims.

Olivine in the cores of the large xenoliths occurs as large (3–5 mm), equant grains that appear to be unaffected by oxidation. Analyses of these grains (analyses 1 and 2, Table 4) yield compositions of Fo_{88}–Fo_{91}. Olivine grains in the xenolith rims have the same size and shape but are typically clouded with an oxidation symplectite (Figs. 3a, b) consisting of magnesioferrite-magnetite (Mt_{58}) intergrown with magnesian enstatite (En_{94}) in a forsterite (Fo_{95}) host (Table 4). In transmitted light, the symplectites appear either as small (0.07 mm) opaque ellipsoidal blebs or, less commonly, as red-brown planar lamellae.

Microprobe analyses of the constituent phases of the bleb-like oxidation symplectites and the olivine grains that host them are given in Table 4 (analyses 9, 10, 11). Descriptions of similar occurrences in terrestrial olivines are reported by Haggerty and Baker (1967), Putnis (1979), and van Lamoen (1979), and references therein.

Figure 3b is a SEM secondary electron image illustrating the opaque magnetite–magnesioferrite ($Mt_{58}Mft_{42}$) rods in a matrix of orthopyroxene (En_{94}). These intergrowths are enclosed by an olivine host that is more forsteritic (Fo_{95}) than the unoxidized olivines in the center of the same lherzolite xenolith. Using Fo_{90} as the composition of original unoxidized olivine, these mineral compositions indicate that the following reaction occurred by the introduction of oxygen to the xenolith rims from an external source:

$$57.2 \ Fo_{90} + O_2 = 50.1 \ Fo_{95} + 3.5 \ En_{94} + 2.3 \ Mft_{42}.$$

The purity of the phases involved is simply an expression of the fact that the phases in the symplectites derive their chemistries from the original unoxidized olivine, which contains very low concentrations of other elements. Although the red-brown lamellae could not be analyzed because of their extreme thinness, it seems likely that they consist of hematite and orthopyroxene, however the possibility that the silicate phase is a silica polymorph cannot be wholly discounted. Hematite derived by oxidation of olivine must be very pure Fe_2O_3 as the Ti necessary to make the $MgTiO_3$ component is not present in the original olivine.

There is no reason to consider the reaction given above as applicable to all symplectite assemblages throughout the xenolith rims. Because the oxidation process is apparently controlled by oxygen diffusion, it is reasonable to assume a gradient in fo_2 and that fo_2 operated as an
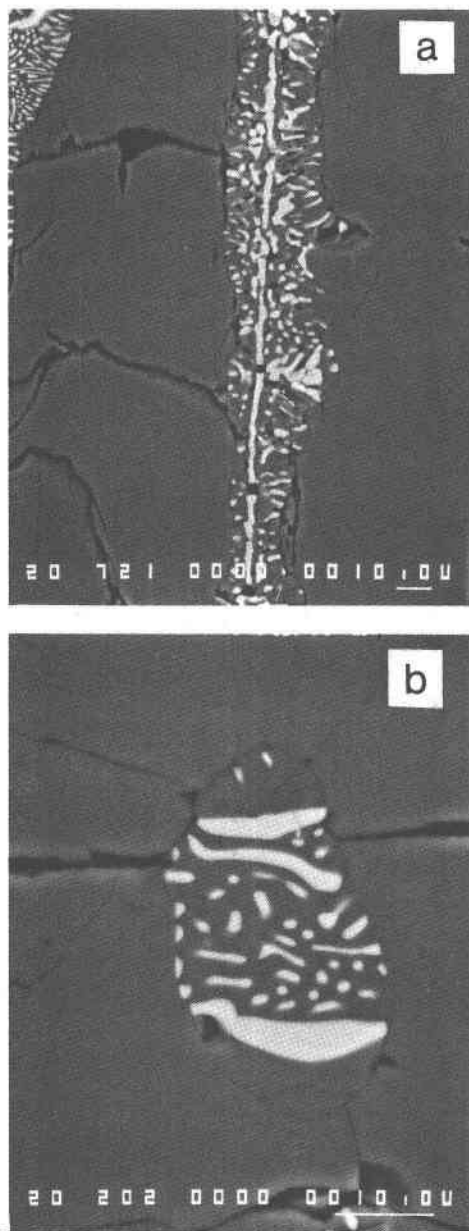
Fig. 3. SEM backscattered electron images of oxidation symplectites in olivine grains in the xenolith rims. The sympletites consist of magnetite–magnesioferrite (white) intergrown with enstatite (grey). Thin cracks surrounding the symplectites separate them from their forsterite hosts. (a) linear symplectite illustrating the control that the host olivine's structure exerts on their orientations. (b) bleb-like symplectite.

independent variable. A temperature gradient may also have existed, but pressure must have been essentially constant across the symplectic xenolith rims. Under these conditions the compositions of coexisting olivine, orthopyroxene and magnesioferrite are dependent only on the fo_2–T–P relations and must become more Fe-rich towards the xenolith interiors. The stoichiometric coeffi-

cients in other balanced reactions, therefore, will be different from those in the equation given above.

Orthopyroxene

Orthopyroxene in the xenolith rims is clouded and darkened by a symplectite consisting of orthopyroxene intergrown with tiny (7 μm wide) interconnected tube-like regions filled with a mixture of probable glass and tiny (2–3 μm) euhedral opaques and olivine. The width of this sieve-like rim on orthopyroxene grains increases toward the margins of the xenoliths, and smaller grains near the xenolith rims are totally consumed by symplectite. Two analyses (analyses 3 and 4, Table 4) of grain interiors not containing the symplectite are given in Table 4. These analyses recalculate to approximately 87 mole% $Mg_2Si_2O_6$ (En), 8% $Fe_2Si_2O_6$ (Fs), and 4% $CaAl_2SiO_6$ (CaTs). Substantial Cr_2O_3 (0.5–0.75 wt.%) is also present. The symplectite textures are very similar to those described by Tracy (1980) in Tahitian nodules.

Clinopyroxene

Aluminous Cr-diopside is a minor phase. Two analyses of interior grains are given in Table 4 (analyses 5 and 6). Both recalculate to En, 46 mole%; Fs, 7%; Wo, 38%; and CaTs, 9%. Cr_2O_3 is substantial (1.1 wt.%) which, with the high CaTs content, is characteristic of high pressure mantle-derived clinopyroxenes.

Cr-spinel

Opaque to blood red Cr-spinel occurs in accessory quantities as large (~3 mm) deeply-embayed grains with quite variable composition. Analyses 7 and 8 (Table 4) are rim and core compositions of a single grain.

Discussion and interpretation

Bulk rock (Table 1) and mineral analyses (Tables 2 and 3) combined with petrographic observations indicate that two closely related but distinct, highly oxidized liquids were involved in the evolution of the Kauai rocks. An early liquid, now the fine-grained groundmass, is intimately associated with a suite of spinel lherzolites against which contacts are generally gradational. A later liquid, now the alkali gabbro, intruded a relatively cool sponge-like aggregate of spinel lherzolite and fine-grained groundmass and subsequently crystallized at relatively shallow depths.

The unusually Mg- and Fe^{3+}-rich mineral chemistries demonstrate that the alkali gabbro and the fine-grained groundmass crystallized from magmatic liquids whose oxygen contents were considerably higher than those normally encountered in igneous rocks. The fact that all phenocryst phases in the alkali gabbro are highly oxidized demonstrates that the melt existed in a highly oxidized state prior to the onset of crystallization and this condition prevailed throughout the entire course of solidification.

Table 4. Microprobe analyses of phases in the cores of lherzolite xenoliths and from the symplectitic xenolith rims

	Analyses from xenolith core								Analyses from sympletitic rim		
	Olivine		Orthopyroxene		Clinopyroxene		Cr-spinel		Olivine	OPX	Spinel
	1	2	3	4	5	6	7	8	9	10	11
SiO_2	41.07	40.69	56.79	54.21	51.23	52.49	0.15	0.05	41.47	57.55	0.20
Al_2O_3	0.00	0.01	2.72	3.97	4.14	3.99	2.52	3.04	0.00	0.11	0.18
TiO_2	0.01	n.d.	0.00	0.10	0.03	0.15	0.52	0.35	n.d.	n.d.	n.d.
FeO[*]	9.29	8.58	5.32	5.67	2.35	2.44	52.36	47.63	5.28	3.57	81.95
MgO	50.19	49.64	33.61	33.29	16.37	16.81	12.01	13.14	52.37	37.28	7.44
MnO	0.16	0.14	0.12	0.18	0.08	0.11	0.25	0.30	0.15	0.08	0.17
CaO	0.11	0.08	0.82	1.03	22.92	21.90	0.07	0.02	0.05	0.14	0.00
Na_2O	0.01	n.d.	0.02	0.07	0.09	0.07	0.00	0.00	n.d.	n.d.	n.d.
Cr_2O_3	0.04	0.03	0.54	0.75	1.14	1.16	26.94	32.44	0.00	0.00	0.08
Total	100.88	99.20	99.93	99.27	98.35	99.12	94.82	96.97	99.33	98.73	90.03
FeO[***]	**	**	**	**	**	**	13.46	12.16	**	**	18.80
Fe_2O[***]	**	**	**	**	**	**	43.23	39.41	**	**	70.17
Total[***]	**	**	**	**	**	**	99.15	100.92	**	**	97.05
Si	0.996	1.000	1.952	1.889	1.894	1.916	0.005	0.002	1.002	1.984	0.008
Al	0.000	0.000	0.110	0.163	0.180	0.172	0.103	0.120	0.000	0.005	0.008
Ti	0.000	n.d.	0.000	0.002	0.001	0.004	0.014	0.009	n.d.	n.d.	n.d.
Fe^{2+}	0.188	0.176	0.153	0.165	0.073	0.074	0.389	0.342	0.107	0.103	0.588
Fe^{3+}	**	**	**	**	**	**	1.124	0.997	**	**	1.974
Mg	1.813	1.817	1.722	1.729	0.902	0.915	0.619	0.658	1.885	1.915	0.415
Mn	0.003	0.003	0.003	0.005	0.002	0.003	0.007	0.009	0.003	0.002	0.005
Ca	0.003	0.002	0.030	0.038	0.908	0.856	0.003	0.001	0.001	0.005	0.000
Na	0.000	n.d.	0.002	0.005	0.007	0.005	0.000	0.000	n.d.	n.d.	n.d.
Cr	0.001	0.001	0.015	0.020	0.033	0.033	0.736	0.862	0.000	0.000	0.002
Cation Total	3.004	3.000	3.987	4.016	4.000	3.978	3.000	3.000	2.998	4.014	3.000
Number of Oxygens	4	4	6	6	6	6	4	4	4	6	4

n.d.: not determined; *: total Fe as FeO; **: not calculated; ***: based on calculated Fe^{2+} and Fe^{3+}.

The basic question remains as to the physicochemical conditions that are responsible for the observed phase assemblages and the mechanism by which these conditions came to exist in the subsurface. We have attempted to bracket the fo_2–T relations represented in the Kauai rocks using two approaches. The first utilizes the empirical expression derived by Sack *et al.* (1980) that allows, provided certain constraints are met, calculation of a curve in fo_2–T space along which a given bulk composition (with known Fe_2O_3 and FeO) is able to exist without changing its Fe^{3+}/Fe^{2+}. Using the bulk rock analyses of the alkali gabbro and the fine-grained groundmass and the equation in Sack *et al.* (1980), we calculated the fo_2–T curves shown in Figure 4. These curves plot approximately two log fo_2 units above the magnetite–hematite buffer (Eugster and Wones, 1962) at all temperatures.

As an alternative, we attempt to bracket the conditions under which the oxidation symplectites in the xenolith rims formed, presuming that these conditions reflect those in the fine-grained groundmass liquid and perhaps in the alkali gabbro as well. This approach offers the advantage that the symplectite assemblage is strictly within the system MgO–FeO–SiO_2–O which has been studied experimentally by Speidel and Osborn (1967). Because the assemblage is trivariant, specification of the compositions of the three phases is sufficient to fix the temperature, fo_2 and the total pressure.

The compositions of the coexisting condensed phases in the assemblage olivine s.s.–orthopyroxene s.s.–magnetite s.s.–gas have been contoured at 1 atm in log fo_2–1/T space by Speidel and Osborn (1967, Fig. 6). By extrapolating their isopleths to more magnesian compositions we estimate that the symplectite assemblage in the rims of the Kauai xenoliths equilibrated at 10^{-3} fo_2 and 1165°C. These equilibration conditions with their estimated uncertainties (due to the extrapolation) are shown on Figure 4. We believe that these conditions represent a lower limit of fo_2 at the stated temperature for the liquid with which the xenoliths attempted to equilibrate. Supporting this interpretation is the presence of Fo_{98} olivine phenocrysts in the alkali gabbro. The experimental work of Speidel and Osborn (1967) and modelling of that data by Nitsan (1974) demonstrate that Fo_{98} olivine is stable at higher fo_2's for the same temperature than the Fo_{95} olivine in the symplectite assemblage. Nitsan's (1974) Fo_{95} olivine isopleth is also plotted in Figure 4 and passes through the symplectite equilibration conditions.

Carmichael and Nicholls (1967) also attempted to estimate the fo_2–T equilibration conditions of the Kauai alkali gabbro using White's (1965) analyses of coexisting Mg–Ti hematite and magnesioferrite and the calibration of Buddington and Lindsley (1964). Carmichael and Nicholls dealt with the problem of minor components by treating Mg as Fe^{2+} and Al as Fe^{3+} in their recalculated Fe–Ti–
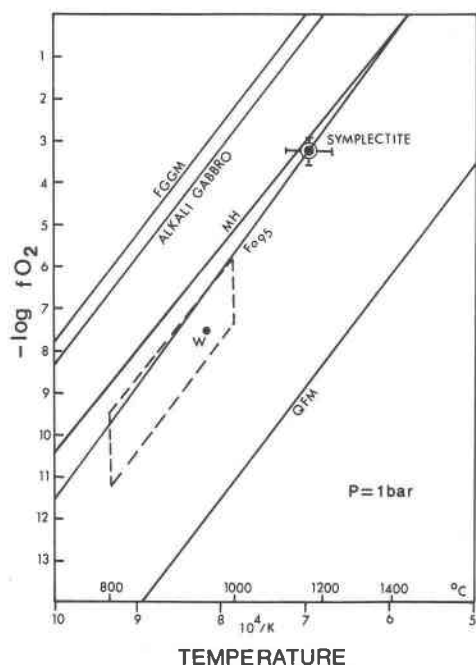
Fig. 4. Log fo_2 vs. $1/T$ relationships for: quartz–fayalite–magnetite buffer (QFM, Eugster and Wones, 1962); Fo_{95} olivine isopleth (Nitsan, 1974); magnetite–hematite buffer (MH, Eugster and Wones, 1962); and the alkali gabbro and the fine-grained groundmass (FGGM), respectively, calculated by the method of Sack *et al*. (1980). Point "W" represents equilibration conditions for the alkali gabbro estimated by Carmichael and Nicholls (1967) and the dashed box is their estimate of the range of conditions under which the rhombohedral and tetragonal Fe–Ti–Mg oxides in the alkali gabbro can coexist. The equilibration conditions of the analyzed oxidation symplectite assemblage in the xenolith rims are also shown (point "S").

Mg–Al oxide analyses. Althugh this procedure is certainly better than ignoring Mg and Al altogether, their calculation of $10^{-7.5}$ fo_2 and 950°C (point 'W', Figure 5) for the Kauai gabbro must be considered an approximation, especially in view of the very magnesian compositions involved (Speidel, 1970; Pickney and Lindsley, 1976; Lindsley and Spencer, 1982). Additionally, they note that this procedure requires considerable extrapolation of Buddington and Lindsley's (1964) data into regions of fo_2–T space not covered in their experiments.

Using the same recalculation scheme along with appropriate experimental data, Carmichael and Nicholls (1967) estimated the range in T–fo_2 conditions under which pseudobrookite s.s. can coexist with hematite s.s. This range is shown as a dashed box in our Figure 4 and in Carmichael and Nicholl's (1967) Figure 5. Because the pseudobrookite s.s. and hematite s.s. occur in the feldspathic groundmass, we agree with Carmichael and Nicholl's interpretation that point W and the dashed box (Fig. 4) represent near solidus equilibration conditions of the alkali gabbro.

The close association of the oxidation symplectite with the fine-grained groundmass in the peripheral regions of the xenoliths suggests that oxidation and partial melting were contemporaneous. It is likely, therefore, that the temperature and fo_2 conditions deduced for the oxidation symplectite are close to those under which melting and the formation of the fine-grained groundmass took place.

Several important and unresolved problems remain. The depths at which the alkali gabbro acquired its unusually high oxygen content, and at which the aggregate of xenoliths and fine-grained groundmass was entrained, are not known. We know only that the oxidizing event(s) was prior to crystallization and prior to incorporation of the xenoliths. The xenoliths had already undergone oxidation and partial melting, presumably by the same mechanism that generated the alkali gabbro elsewhere in the mantle. If the alkali gabbro represents the sole host for its entrained xenoliths, it then seems highly probable that the oxidation and melting mechanisms were operative in the mantle below Kauai at depths greater than about 10–12 km.

The mechanism by which the relatively high oxygen fugacity of the alkali gabbro was attained in the wholly magmatic state is also unknown. It seems improbable that the process involves interaction with meteroric or sea water because of the vast amounts required in solution to significantly raise fo_2 (Gerlach and Nordlie, 1975b). Moreover, the virtual absence of hydrous phases in the now crystallized alkali gabbro indicates little dissolved water in the original melt.

A more plausible explanation is to invoke processes which operate entirely within the melt. One possibility proposed by Sato and Wright (1966), Wright and Okamura (1977), and Watkins and Haggerty (1967) involves the diffusion of H_2 out of the rock and the subsequent increase of O_2. This mechanism presumably operates in the subsolidus at temperatures well below those inferred for the alkali gabbro melt. Another possibility would be to deplete a coexisting gas phase in sulfur, for example, by crystallizing an early sulfide phase from the magma. A similar oxidizing effect results due to the magma-gas equilibria (Gerlach and Nordlie, 1975b). Isotopic studies are now in progress to resolve some of these possibilities.

Acknowledgments

References

Akasaka, M. and Onuma, K. (1980) The join $CaMgSi_2O_6$–$CaFeAlSiO_6$–$CaTiAl_2O_6$ and its bearing on the Ti-rich fassaitic pyroxenes. Contributions to Mineralogy and Petrology, 71, 301–312.

Anderson, A. T. (1968) The oxygen fugacity of alkaline basalt and related magmas, Tristan de Cunha. American Journal of Science, 266, 704–727.

Bell, P. M. and Mao, H. K. (1971) A study of ferric and ferrous ions in three natural pyroxenes and one synthetic pyroxene: Crystal field determinations of Fe^{3+}. Carnegie Institution of Washington Yearbook, 71, 528–533.

Boivin, P. (1980) Données expérimentales préliminaires sur la stabilité de la rhônite à 1 atmosphère. Application aux gisements naturels. Bulletin de Mineralogie, 103, 491–502.

Brady, J. B. and Stout, J. H. (1980) Normalizations of thermodynamic properties and some implications for graphical and analytical problems in petrology. American Journal of Science, 280, 173–189.

Buddington, A. F. and Lindsley, D. H. (1964) Iron–titanium oxide minerals and synthetic equivalents. Journal of Petrology, 5, 310–357.

Cameron, K. L., Carman, M. F., and Buttler, J. C. (1970) Rhönite from Big Bend National Park, Texas. American Mineralogist, 55, 864–874.

Carmichael, I. S. E. and Nicholls, J. (1967) Iron–titanium oxides and oxygen fugacities in volcanic rocks. Journal of Geophysical Research, 72, 4665–4687.

Deer, W. A., Howie, R. A., and Zussman, J. (1978) Rock Forming Minerals, Vol. 2A, Single-Chain Silicates, Wiley, New York.

Eugster, H. P. and Wones, D. R. (1962) Stability relations of the ferruginous biotite, annite. Journal of Petrology, 3, 82–125.

Finger, L. W. (1972) The uncertainty in calculated ferric iron content of a microprobe analysis. Carnegie Institution of Washington Yearbook, 71, 600–603.

Gerlach, T. M. and Nordlie, B. E. (1975a) The C–O–H–S gaseous system, part I: composition limits and trends in basaltic cases. American Journal of Science, 275, 353–376.

Gerlach, T. M. and Nordlie, B. E. (1975b) The C–O–H–S gaseous system, part II: temperature, atomic composition and molecular equilibria in volcanic gases. American Journal of Science, 275, 377–394.

Grandclement, J. (1980) Conditions de synthèse et de stabilité de la rhônite. Ph.D. Thesis, L'Université de Poitiers, Poitiers, France.

Greenwood, H. J. (1975) Thermodynamically valid projections of extensive phase relations. American Mineralogist, 60, 1–8.

Haggerty, S. E. (1976) Opaque mineral oxides in terrestrial igneous rocks. In, D. Rumble III, ed., Oxide Minerals, Mineralogical Society of America Short Course Notes 3, Hg101–Hg300.

Haggerty, S. E. and Baker, I. (1967) The alteration of olivine in basaltic and associated lavas, part I: high temperature alteration. Contributions to Mineralogy and Petrology, 16, 233–257.

Lindsley, D. H. and Spencer, K. J. (1982) Fe-Ti oxide geothermometry: reducing analyses of coexisting Ti magnetite (Mt) and ilmenite (Ilm). Transactions of the American Geophysical Union, 63, 471.

MacDonald, G. A. (1968) Composition and origin of Hawaiian lavas. Geological Society of America Memoir 116, 447–522.

MacDonald, G. A., Davis, D. A., and Cox, D. C. (1960) Geology and groundwater resources of the island of Kauai, Hawaii. Hawaii Division of Hydrography Bulletin 13.

Magonthier, M. C. and Velde, D. (1976) Mineralogy and petrology of some Tertiary leucite–rhonite basanites from Central France. Mineralogical Magazine, 40, 817–826.

Marfunin, A. S. (1979) Physics of Minerals and Inorganic Materials: an Introduction. Springer-Verlag, New York.

Nitsan, Uzi (1974) Stability field of olivine with respect to oxidation and reduction. Journal of Geophysical Research, 79, 706–711.

O'Nions, R. K. and Pankhurst, R. J. (1974) Petrogenetic significance of isotope and trace element variations in volcanic rocks from the mid-Atlantic. Journal of Petrology, 15, 603–634.

Onuma, K., Akasaka, M., and Yagi, K. (1981) The bearing of the system $CaMgSi_2O_6$–$CaAl_2SiO_6$–$CaFeAlSiO_6$ on fassaitic pyroxene. Lithos, 14, 173–182.

Palmiter, D. B. (1975) The Geology of the Koloa Volcanic Series of the South Coast of Kauai, Hawaii. M.S. Thesis, University of Hawaii, Honolulu.

Pickney, L. R., and Lindsley, D. H. (1976) Effects of magnesium on iron-titanium oxides. (abstr.) Geological Society of America Abstracts with Program, 8, 1051.

Powell, M. (1978) Crystallization conditions of low-pressure cumulate nodules from the Lesser Antilles arc. Earth and Planetary Science Letters, 39, 162–172.

Putnis, A. (1979) Electron petrography of high-temperature oxidation in olivine from the Rhum Layered Intrusion. Mineralogical Magazine, 43, 293–296.

Sack, R. O., Carmichael, I. S. E., Rivers, M., and Ghiorso, M. S. (1980) Ferric–ferrous equilibria in natural silicate liquids at 1 bar. Contributions to Mineralogy and Petrology, 75, 369–376.

Sato, M. (1972) Intrinsic oxygen fugacities of iron-bearing oxide and silicate minerals under low total pressure. Geological Society of America Memoir 135, 289–307.

Sato, M. and Wright, T. L. (1966) Oxygen fugacities directly measured in volcanic gases. Science, 153, 1103–1105.

Sigurdsson, H. and Brown, G. M. (1970) An unusual enstatite-forsterite basalt from Kolbeinsey Island, north of Iceland. Journal of Petrology, 11, 205–221.

Speidel, D. H. (1970) Effect of magnesium on the iron–titanium oxides. American Journal of Science, 268, 341–353.

Spiedel, D. H. and Osborn, E. F. (1967) Element distribution among coexisting phases in the system MgO–FeO–Fe_2O_3–SiO_2 as a function of temperature and oxygen fugacity. American Mineralogist, 52, 1139–1152.

Stout, J. H. and Johnston, A. D. (1980) Natural partial melt asemblages in spinel lherzolites. (abstr) Transactions of the American Geophysical Union, 61, 1143.

Tracy, R. J. (1980) Petrology and genetic significance of an ultramafic xenolith suite from Tahiti. Earth and Planetary Science Letters, 48, 80–96.

van Lamoen, Hans (1979) Coronas in olivine gabbros and iron ores from Susimaki and Riuttamaa, Finland. Contributions to Mineralogy and Petrology, 68, 259–268.

von Knorring, O. and Cox, K. G. (1961) Kennedyite, a new mineral of the pseudobrookite series. Mineralogical Magazine, 32, 676–682.

Watkins, N. D. and Haggerty, S. E. (1967) Primary oxidation variation and petrogenesis in a single lava. Contributions to Mineralogy and Petrology, 15, 251–271.

White, R. W. (1965) Ultramafic Inclusions in Basaltic Rocks from Hawaii. Ph.D. Thesis, University of California, Berkeley.

Wright, T. L. and Okamura, R. T. (1977) Cooling and crystallization of tholeiitic basalt, 1965 Makaopuhi Lava Lake, Hawaii. U.S. Geological Survey Professional Paper 1004.